The Role of Molecular Layering in the Enhanced Mechanical Properties of Stable Glasses

Sarah E. Wolf,[†] Sage Fulco,[‡] Aixi Zhang,[†] Haoqiang Zhao,[†] Patrick J. Walsh,[†] Kevin T. Turner,[‡] and Zahra Fakhraai*,[†]

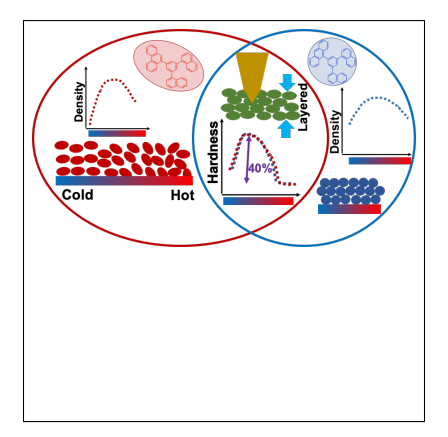
†Department of Chemistry, University of Pennsylvania, Philadelphia, PA ‡Department of Mechanical Engineering and Applied Mechanics, University of Pennsylvania, Philadelphia, PA

E-mail: fakhraai@sas.upenn.edu

Abstract

The density, degree of molecular orientation, and molecular layering of vapor-deposited stable glasses (SGs) vary with substrate temperatures (T_{dep}) below the glass transition temperature (T_g). Density and orientation have been suggested as factors influencing the mechanical properties of SGs. We perform nanoindentation on two molecules which only differ by a single substituent, allowing one molecule to adopt in-plane orientation at low T_{dep} . The reduced elastic modulus and hardness of both molecules show similar T_{dep} -dependence, with an enhancement of 15-20% in reduced modulus and 30-45% in hardness at $T_{dep} \sim 0.8T_g$, where the density of vapor-deposited films are enhanced by $\sim 1.4\%$ compared to the liquid-quenched glass. At $T_{dep} < 0.8T_g$, one of the molecules produces highly unstable glasses with in-plane orientation. However, both systems show enhanced mechanics. Both modulus and hardness correlate with the degree of layering, which is similar in both systems despite their variable stability. We suggest that nanoindentation performed normal to the film's surface is influenced by the tighter packing of the molecules in this direction.

TOC Graphic



Keywords

Stable Glass, Physical Vapor Deposition, Mechanical Properties, Nanoindentation, Molecular Layering, Structural Anisotropy

Physical Vapor Deposition (PVD), under the right deposition conditions, can produce highly stable glasses on laboratory timescales, that are analogous to glasses aged for hundreds or millions of years. ^{1–5} In this process, the glass-former of interest is thermally deposited under vacuum conditions onto a substrate held below the glass transition temperature (T_g), while both substrate deposition temperature (T_{dep}) and the deposition rate (T_{dep}) are controlled. Since their discovery, ¹ significant work has been devoted to exploring the unique properties of these stable glasses. ^{5,7–11} Stable glasses (SGs) have lower enthalpy, ¹ higher density, ⁵ and improved kinetic stability ⁶ when compared to ordinary (liquid-quenched) glasses.

Unlike most liquid-quenched glasses, vapor-deposited molecular glasses can show significant structural and optical anisotropy. ^{12–14} Anisotropy is also observed in properties such as thermal conductivity ¹⁵ and mechanical properties. ¹⁶ Anisotropy in PVD glasses has been primarily attributed to the preferred orientation of molecules at the free surface. ^{9,13,17–22} However, optical birefringence has also been observed in vapor-deposited glasses without any molecular orientation. ¹⁴ Such structural anisotropy, independent of molecular orientation, has been attributed to molecular layering normal to the film's surface. ^{9,14,23–26} Molecular layering is directly observed in grazing incidence wide-angle X-ray scattering (GIWAXS) experiments as a unique scattering peak in the out of plane direction. ^{23,26}

Molecular orientation and layering emerge due to the surface-mediated equilibration and accelerated aging processes. The surface region of glasses have enhanced mobility and lower T_g values. $^{25,27-29}$ During PVD, surface molecules can equilibrate and age at an accelerated rate, 25,27 the rate of which is controlled through the deposition temperature (T_{dep}) and deposition rate (T_{dep}). As such. the structure and dynamics of the glass is influenced by that of this liquid-like layer at the free surface boundary. Deposition close to T_g and at slower T_{dep} results in isotropic and near-equilibrium states, while lower T_{dep} and faster T_{dep} can result in preferred molecular orientation and layering. Generally a T_{dep} - T_{dep} superposition rule can be established for the structural anisotropy at other properties of PVD glasses. Simulations have shown that a molecule's orientation can strongly vary with its depth from the free surface, which in turn depends on the time

allowed for the molecule to equilibrate below the immediate free surface.^{24,32} If the surface mobility is limited to one layer, in-plane orientation is templated throughout the film, while relaxation below the surface can result in out of plane²² or isotropic³² orientation.

While the specific origins of molecular layering are unknown, our previous studies in a spherically-shaped molecular glass, 9-(3,5-di(naphthalen-1-yl)phenyl)anthracene (α , α -A), has shown a strong correlation between this feature and increased index of refraction in the direction normal to the film surface (vertical direction). ^{14,25} As such we have interpreted this feature to be indicative of tighter packing of molecules in this direction. Furthermore, our recent experimental data suggests that layering likely emerges due to accelerated rate of aging the near-surface. ²⁵ As the surface molecules fall out of equilibrium upon further deposition, they can still age rapidly, ²⁷ while being constrained by the rigid out of equilibrium regions of the film. The influence of the free surface structure in templating anisotropy is also evident in vapor deposition of liquid crystalline (LC) molecules, which can adopt highly tunable LC phases that are not observed in liquid-quenched states. ^{21,33} The tunability of the structure of both liquid crystals and molecular glasses through PVD makes them attractive candidates for applications where orientation and anisotropy are important.

Chemical structure can be used to tune the structural features in stable glasses. Strong intermolecular interactions such as hydrogen bonding ^{29,34–36} can influence the free surface mobility and reduce the degree of stability, while other chemical motifs can produce microphase-separated states. ³² In a recent study, we demonstrated that intra-molecular relaxations can be varied to modify the equilibrium shape of a molecule, which can then influence their degree of stability upon PVD, by affecting the liquid structure and mobility of the mobile surface layer. ^{25,37}

The specific role of stability and anisotropic structure on the mechanical properties of vapor-deposited glasses remains relatively under-studied. Previously, Brillouin Light Scattering measurements showed higher elastic moduli and sound velocity in SGs compared to liquid-quenched glasses, ^{12,16,38} and indicated anisotropy in these properties. ¹⁶ Nanoindentation experiments have also been employed to show increased hardness and modulus with increased degree of stability. ³⁹ This study suggested that the change in the hardness is well-correlated with the change in the den-

sity of a stable glass film, while the change in modulus was found to correlate with the optical birefringence. Wrinkling experiments were also employed to measure the modulus of thin PVD films, indicating that besides the substrate temperature, the film thickness can also influence the value of modulus. ^{8,40}

In this study, we use nanoindentation to measure the mechanical properties of vapor-deposited glasses of two isomeric organic molecules with similar bond connectivity, but different molecular shapes. 25,37 To obtain reliable nanoindentation data, we correct for surface detection errors in nanoindentation experiments, which are caused by the soft surface of these glasses. $^{41-43}$ Corrected values of the reduced modulus and hardness are obtained by modifying both indentation procedures and data analysis, based on our recently developed methods. 43 We find enhanced mechanical properties in the most stable glasses of these molecules ($T_{dep} \sim 0.8T_g$), on the order of 30-45% for hardness and 15-20% for reduced modulus, compared to glasses deposited at T_g . Measurements on a broad range of deposition temperatures indicates that while the degree of enhancement correlates with the enhancement in density when T_{dep} is close to T_g , the enhancement in the modulus and hardness are beyond that predicted by density at low deposition temperatures ($T_{dep} < 0.8T_g$). The degree of enhancement in these molecules are also independent of their molecular orientation. Instead, we observe a strong correlation between mechanical properties and molecular layering, interpreted as tighter molecular packing in the vertical direction, and therefore better mechanical enhancement in the direction of indentation.

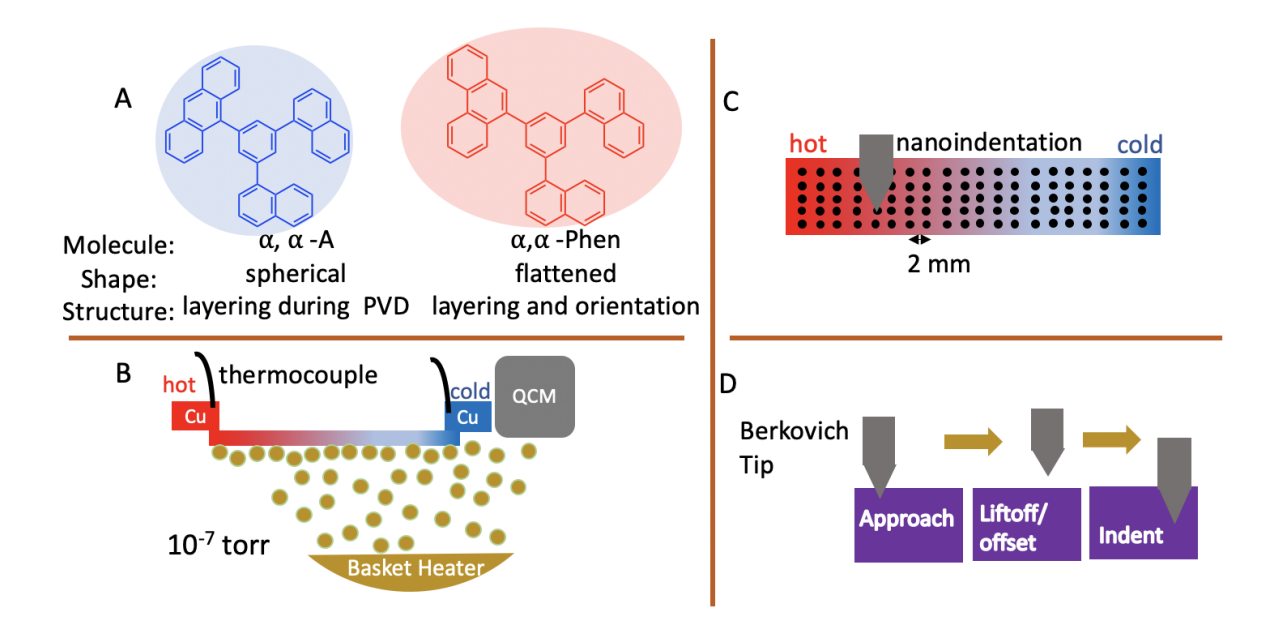


Figure 1: Schematic of the experimental approach. A) The structures of the two molecules used in this study: 9-(3,5-di(naphthalen-1-yl)phenyl)anthracene (α , α -A), and 9-(3,5-di(naphthalen-1-yl)phenyl)phenanthrene (α , α -Phen). B) A schematic of the vapor deposition setup and the substrate's deposition temperature gradient (T-grad). C) Schematics of the nanoindentation patterns used on T-grad samples for high-throughput experiments. The color gradient demonstrates the gradient of T_{dep} values, while the patterns show points along the sample where nanoindentation was performed at room temperature. D) The nanoindentation procedure at each point; approach, liftoff, lateral offset, and indentation, used to avoid surface detection errors. 43

Detecting the True Surface. Figure 1 shows the molecular structures of 9-(3,5-di(naphthalen-1-yl)phenyl)anthracene (α , α -A), and 9-(3,5-di(naphthalen-1-yl)phenyl)phenanthrene (α , α -Phen) molecules and an outline of the methods used in this study. Samples were prepared by physical vapor deposition and investigated by a modified nanoindentation approach. More details can be found in the Materials and Methods section and Supporting Information (SI). Figures 2A and C show examples of load versus displacement curves obtained for α , α -Phen and α , α -A samples, respectively. As can be seen, the load increase starts at a point \sim 20 nm above the apparent detected surface, meaning that the initially detected surface by the instrument is about 20 nm below the true

surface of the sample. To correct these load-displacement curves, the correct location of the surface was identified as the point where the load increased above the baseline in-air values. The curves were then shifted both horizontally and vertically, such that the in-air load values were on average zero, and the point at which the load increased beyond the baseline was identified as the zero displacement, *i.e.* the true surface location (shown with dashed lines in figures 2B and C). More details of this approach can be found in the SI. The corrected curves for the data in Figures 2A and C, based on this approach are shown in Figures 2B and D, respectively.

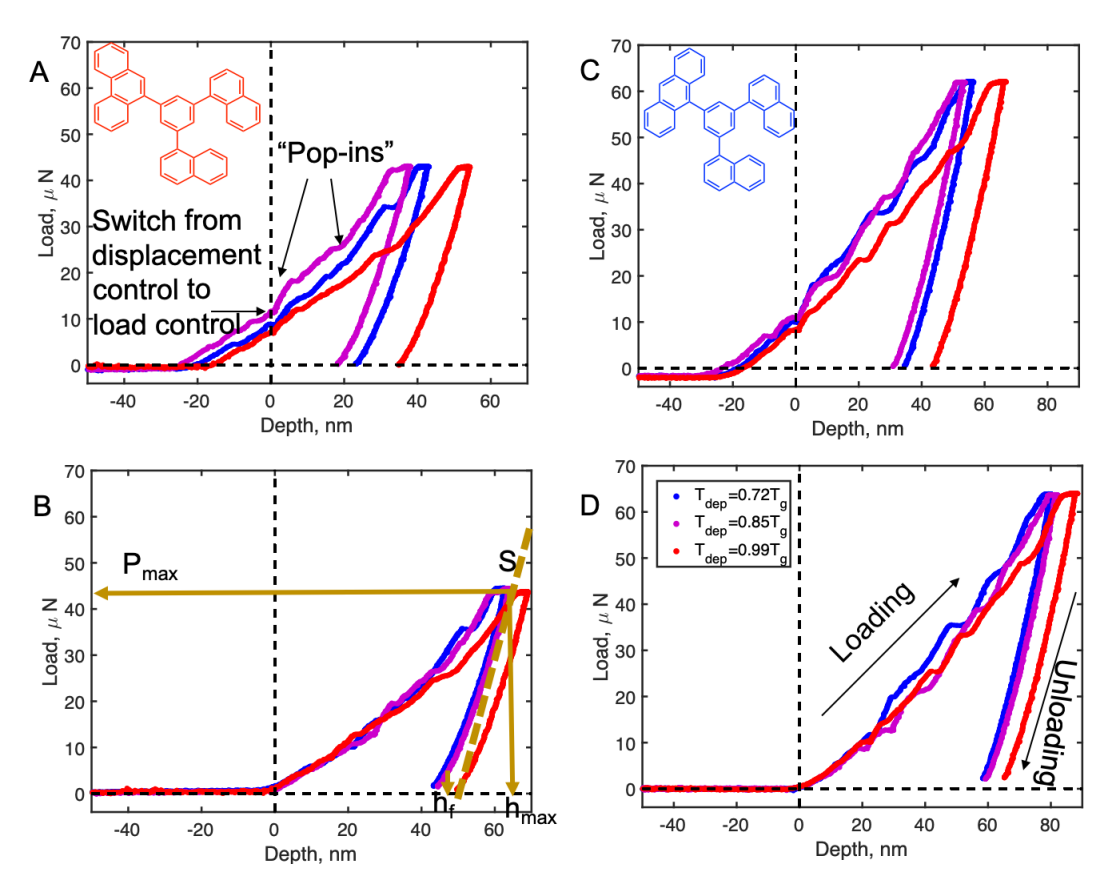


Figure 2: A) Examples of load-displacement curves for α , α -A samples at three different deposition temperatures, $T_{dep}=260~{\rm K}~(0.72T_g,$ blue), 307 K (0.85 T_g , purple), and 357K (0.99 T_g , red). The inset shows the molecule's structure. B) The corrected load-displacement curves after accounting for the surface detection error. Inset demonstrates the value of P_{max} , h_{max} , the slope S, and the final indentation depth (h_f) for the data at $T_{dep}=0.85T_g$. C) Examples of load-displacement curves for α , α -Phen samples at different deposition temperatures, $T_{dep}=261~{\rm K}~(0.72T_g,$ blue), 308 K (0.85 T_g , purple), and 359 K (0.99 T_g , red). The inset shows the molecule's structure. D) The corrected load-displacement curves after accounting for the surface detection error. The arrows show the direction of loading and unloading in all figures. The relative T_{dep} values shown in the legend apply to all four plots.

Nanoindentation Analysis. Figures 2B and D show the load-displacement curves at various T_{dep} for α, α -Phen and α, α -A molecules, after corrections are applied to account for surface detection errors. We note that these loading curves are noticeably less smooth than may be expected in typical nanoindentation experiments. In all curves, a flat region can be observed around the machine-determined apparent surface (indicated by an arrow in Figure 2A). This is a systematic error due to a switch from displacement control during the approach to load control the moment the surface is detected. During this swap, there is a brief (1 second) pause by the instrument, which causes a small amount of creep to occur before load-controlled indentation begins. Given the error in surface detection, this point occurs at a displacement of \sim 20 nm instead of the actual surface. However, there is no reason to suspect this feature impacts the results reported here. In addition to this feature, random "pop-ins" are also observed at higher load values throughout the loading region. These pop-ins are attributed to the brittle nature of these films, which can result in shear transformations. ⁴⁴ Due to limited data on these features, they are not further analyzed in this study.

The data presented in Figures 2B and D also show that for each molecule, the loading curves are different at different T_{dep} values, indicating a dependence of the mechanical properties on the deposition temperature. For example, the load-displacement curves for $T_{dep} \sim T_g$ for both molecules (red curves in Figures 2B and C) show a higher displacement at the same maximum load compared to data at other T_{dep} values, suggesting lower hardness. This is consistent with the fact that deposition below T_g yields more stable glasses with higher density. ^{25,37} The difference in maximum load between different samples in Figures 2 A and C is to maintain a maximum depth of less than 10% of the total film thickness, which was slightly different between these two samples. This maximum indentation range was chosen to avoid an influence of the substrate on the measurements. Figure S1 of SI shows that within the range of depths used in this study for various samples and various deposition temperatures, and within the scatter of the data, there is no dependence of the measured values on the maximum indentation depth, confirming that substrate effects are negligible.

Measurements of modulus and hardness were obtained from the nanoindentation data using the

Oliver-Pharr method. The unloading portion of the curve was fit to a power-law equation:

$$P = \alpha (h - h_f)^m \tag{1}$$

Where P is the load, h is the indentation depth and h_f is the final displacement depth (at zero load), and α and m are fitting parameters, with $1.2 \le m \le 1.6$ (more details in SI). The data points were weighted according to their location on the unloading curve, with a weighting of 95% on the upper portion (high load) and 20% on the lower portion (low load) of the unloading curve. This was based on typical weighting used by the commercial (Hysitron) nanoindenter software. This weighting is used because the initial slope of the unloading curve is more important in determining the values of hardness and modulus. To determine the value of the elastic unloading stiffness (S), the derivative of this power-law equation was averaged over the initial region of the unloading curve (typically 15 data points). Hardness (H) and nanoindentation reduced modulus (E_r) were then determined using equations 2 and 3, as detailed in SI:

$$H = \frac{P_{max}}{A} \tag{2}$$

$$E_r = \frac{S\sqrt{\pi}}{2\beta\sqrt{A}}. (3)$$

Here, β is a constant that depends on the tip-geometry ($\beta = 1.034$ for Berkovich tips) and A is the projected area of the tip at the peak contact depth. It is also possible to determine S by fitting a line to the initial, linear region of the unloading curve. This fitting was also performed and the data was compared with S determined through the power-law fitting. If these two values were different by more than 15% for a particular load-displacement curve, that data point was not used for subsequent analysis. Very few points were rejected as a result of this approach, leaving at least 20 independent load-displacement curves, for which the data was collected and averaged at each deposition temperature. In situations where fewer data points were available (for example, where a sample had dust particles or other surface contaminations), the data was not used for a given T_{dep} .

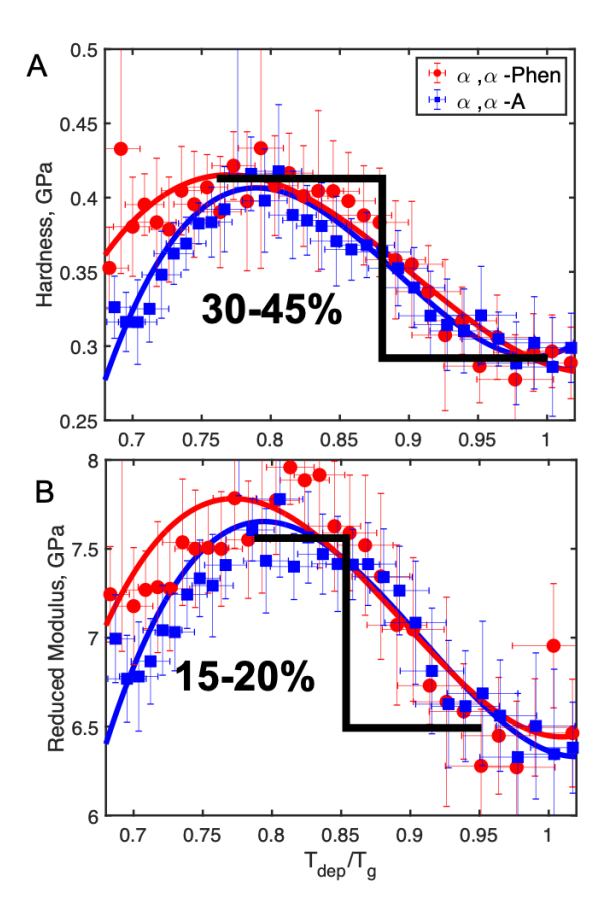


Figure 3: A) Hardness and B) reduced elastic modulus of α , α -A (blue) and α , α -Phen (red) as a function of deposition temperature, normalized by T_g (T_{dep}/T_g) of each molecule. Solid lines represent a polynomial fitting to each curve to guide the eye. The black lines in each curve highlight the approximate relative increase in the hardness (30-45%) and reduced modulus (15-20%) at maximum (near $T_{dep} \sim 0.8T_g$) compared to the corresponding values at $T_{dep} = T_g$.

Dependence of Mechanical Properties on the Deposition Temperature. Figure 3A and B show the hardness and reduced modulus as a function of T_{dep} for both glasses. In both systems, a strong T_{dep} -dependence is observed. As T_{dep} is decreased, H and E_r increase dramatically, reaching a maximum around $T_{dep} \sim 0.8T_g$ for both systems. In both systems, significant improvements in mechanical properties are observed, with 30-45% increase in hardness and 15-20% increase in the reduced modulus in the deposition temperature range of $0.78T_g - 0.82T_g$ (as compared to the deposition temperature range of $0.98T_g - 1.02T_g$). This is a larger enhancement in mechanical properties than previously observed for other stable glass systems measured via nanoindentation. ³⁹ As the deposition temperature is further decreased, both hardness and reduced modulus start de-

creasing. However, both values remain higher than their corresponding values at $T_{dep} = T_g$ for the entire range of T_{dep} accessible in this study.

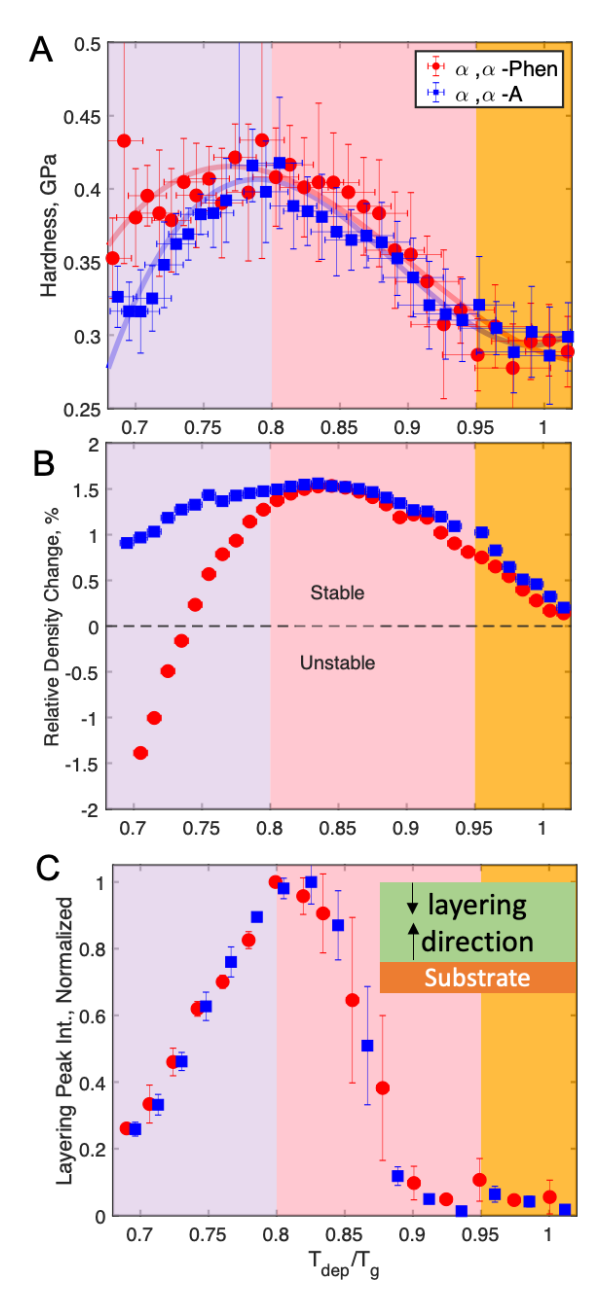


Figure 4: (A) Hardness, (B) relative density change, and (C) normalized layering peak intensity as a function of deposition temperature, normalized to T_g , for α , α -A (blue) and α , α -Phen (red). Colored shading highlights three proposed regimes as described in the main text.

Dependence of Mechanical Properties on the Glass Structure. A surprising aspect of the data presented in Figure 3 is the fact that the temperature-dependence and the absolute values of both hardness and reduced modulus at each T_{dep} are nearly the same in both molecular glasses to within the scatter of the data. We have recently shown that there is a significant difference in the structure and stability of vapor-deposited films of these two molecules, stemming from the differences in their molecular shape and flexibility, which affects the details of their free surface equilibration rate at low T_{dep} . ^{25,37}

To understand this phenomenon, in Figure 4 we plot hardness alongside relative density change $(\Delta\rho)$ and normalized layering peak intensity, as reported in our previous publication. ²⁵ We first focus on the high- T_{dep} region $(0.95T_g < T_{dep} < T_g)$, highlighted in orange). In this region, the density increases by $\Delta\rho \sim 0.5\%$ as T_{dep} is decreased (Figure 4B), and the vapor-deposited glass is isotropic, with near zero optical birefringence (Figure S3 of SI) and no layering (Figure 4C). This is consistent with the fact that in most PVD glasses the thermal stability, as measured here through the density, typically follows the extrapolated equilibrium values of the supercooled liquid, ^{45,46} and the glass is isotropic, indicative that it is reaching near-equilibrium states. Surprisingly, in this region, both hardness and reduced modulus, measured through nanoindentation, remain unchanged within the scatter of the data (Figure 4A).

As the deposition temperature is further reduced $(0.8T_g < T_{dep} < 0.95T_g$, pink region) the density continues to increase in both systems (Figure 4B), roughly following the same temperature-dependence as the high T_{dep} region. In this regime, both molecules show a positive birefringence, which is reflective of the emergence of molecular layering. The layering in this region is directly observed in GIWAXS experiments, where a distinct peak is observed in the out-of-plane scattering direction (Figure S2). The intensity of this peak grows as the temperature is decreased. Though the absolute extent of layering is slightly different in these molecules (Figure S3B), which is also reflected in the values of their optical birefringence, the temperature-dependence of the layering, as measured through the normalized peak intensity, is similar for both glassformers. Both hardness and modulus dramatically increase in this region such that the density increase of $\Delta \rho \sim 1.4\%$

relative to the glass deposited at T_g corresponds to a relative harness increase of $\Delta H \sim 30\text{-}45\%$ and a relative increase of the reduced modulus by $\Delta E_r \sim 15\text{-}20\%$ within the scatter of the data obtained at various locations of indentation. This dramatic increase in the mechanical properties correlates well with the extent of layering, as measured by the normalized layering peak intensity (Figure 5), and a reasonable correlation is also observed with the increased density in this range of T_{dep} . However, a poor correlation is seen with either density or birefringence when the entire range of T_{dep} is considered (Figure S4 of SI).

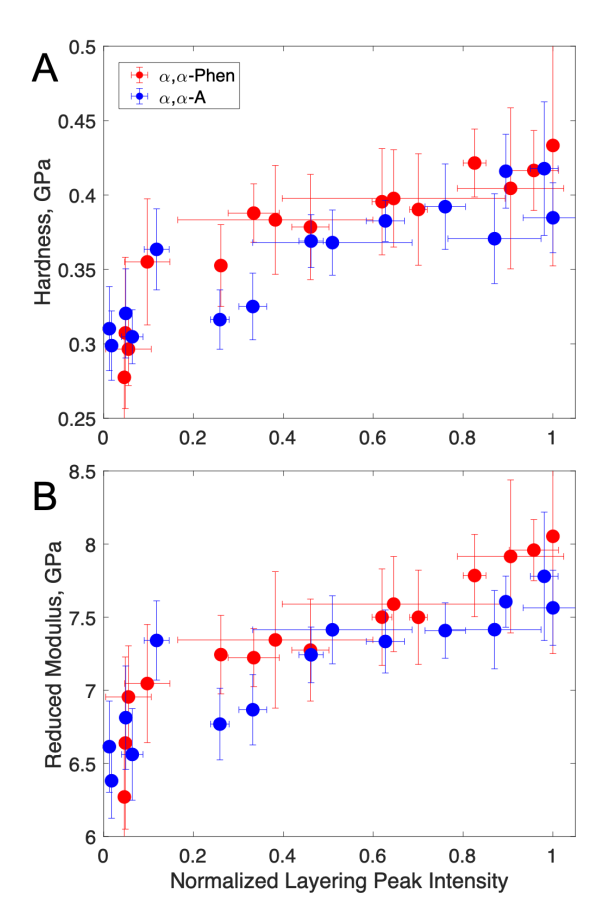


Figure 5: Correlation plots of A) hardness and B) reduced modulus with the normalized layering peak intensity for α , α –A (blue) and α , α –Phen (red) molecules.

Both hardness and modulus continue to remain correlated with the layering peak intensity even for $T_{dep} < 0.82T_g$, where vapor-deposited glasses are in kinetically trapped states (Figure 5), and their stability is reduced. Notably, in α , α -Phen, deposition below $0.75T_g$ results in unstable films with density values below that of the liquid-quenched glass (Figure 4B), while α , α -A

glasses have improved density and stability in this region. Similarly, the degree of optical bire-fringence is significantly different in this region (Figure S3A). In α , α -Phen, these aspherical molecules assume an in-plane orientation, 25,37 which yields negative values of birefringence, while spherically-shaped α , α -A molecules remain isotropic. 14,25 Despite these significant differences in orientational order and stability of glasses deposited at $T_{dep} < 0.8T_g$, their hardness and modulus are nearly the same, and significantly higher than their corresponding values when deposited at T_g . We note that the intensity of the layering peak also remains non-zero in this region with strong correlations with hardness and modulus (Figure 5).

These observations are in contrast to previous work in vapor-deposited glasses of N,N'- bis(3methylphenyl)-N,N'-diphenylbenzidine (TPD)³⁹ where it was reported that the hardness is correlated with density across the reported range of deposition temperatures, while modulus was found to relate to the molecular orientation. A comparison with molecular layering was not provided in that study. Previous Brillouin light scattering experiments in indomethacin stable glasses had also shown a strong dependence of the longitudinal sound velocity on T_{dep} , 38 which correlates well with the density in the equilibrium region of the T_{dep} curve. 46 However, this correlation breaks at low T_{dep} similar to the data shown here. While a correlation with the layering peak intensity was not made in these studies, the speed of sound remains higher than predicted by density at low T_{dep} where the layering peak intensity is also non-zero. ^{26,46} It is important to note that α, α -A is spherical and thus its positive birefringence is due to layering as opposed to orientation. 14,25 While α, α -Phen is ashperical, and is able to take an in-plane orientation at low T_{dep} , its degree of asphericity is small²⁵ compared to the elongated molecules used in previous nanoindentation studies. 39 As such, at high values of T_{dep} its measured birefringence has more contribution from layering than out of plane orientation. It is possible that the mechanical properties of molecules with stronger orientational anisotropy would be more strongly influenced by their orientational order.

Here, given the unique structure of the designed molecules, we can separate the effects of layering and in-plane molecular orientation, both of which affect the measured optical birefringence. ^{9,25}

While the exact details of molecular layering remains unknown, when normalized against maximum intensity (Figure 4C), the temperature-dependence of this peak follows the same trend, which appears to be the most prominent factor in the enhanced mechanical properties measured in nanoindentation experiments. As noted above, it is possible that when a more anisotropically-shaped molecule is used, both orientation and layering can affect the nanoindentation data.

We note that molecular layering and its corresponding peak in GIWAXS experiments are always observed in the direction normal to the film's surface (Figure S2). It has been hypothesized that this is due to the fact that at these cold deposition temperatures, the molecules at the near surface region have fallen out of equilibrium, and while their dynamics are still enhanced compared to the rest of the film, their relaxation is due to enhanced rate of physical aging. The lateral constraint imposed by the glassy layer below the free surface prevents density increases in the lateral direction, while the molecules can still adopt closer packing in the vertical direction. ¹⁴ Nanoindentation is also performed by indenting the tip in the direction normal to the surface. As such, it is not surprising that the measured quantities in this direction are influenced by this distinct layering structure.

Previous reports have indeed shown that stable glasses exhibit significant anisotropy in their elastic properties, ^{12,16} due to their structural anisotropy. Nanoindentation experiments in anisotropic materials measure a reduced modulus that is a complex function of moduli in all directions, with the direction of indentation providing the main contribution. ⁴⁷ Through the methods used in this study, separation of the directional moduli is not possible because we do not have access to the corresponding in-plane values. However, we use the computed "indentation modulus" as an effective modulus which remains valuable in our comparisons. The potential for nanoindentation to probe anisotropic materials has been explored in depth, ^{47–51} in particular for indenters of simple symmetry and by doing indentations in multiple directions, but these methods are not possible for the thin film samples in this work. Future work may include probing mechanics in other directions. The current work suggests that nanoindentation may be a unique method to explore layering properties.

In summary, we demonstrate that accurate surface detection is critical in obtaining correct

nanoindentation data in soft molecular glass systems. Accounting for this, we find that mechanical properties are significantly improved in vapor-deposited glasses of two structurally similar molecules. A 30-45% increase in hardness and 15-20% increase in reduced modulus is measured in the most stable glasses of both molecules, deposited around $0.8T_g$. When PVD is performed near T_g , where near-equilibrium structures are produced, both hardness and modulus correlate reasonably well with the glass density. At low deposition temperatures, kinetically trapped structures are formed. In this regime, hardness and modulus are found to be improved even for glasses that are unstable and have significantly lower density than the bulk glass. In both systems over the entire range of deposition temperatures the mechanical properties correlate well with molecular layering, which indicates tighter molecular packing in the direction of deposition/indentation. We do not observe a correlation between molecular orientation and mechanical properties as measured by nanoindentation. Given the strong correlation between nanoindentation properties and layering, nanoindentation can be considered as an alternative approach to probe the degree of layering in vapor-deposited glasses of other molecules, which can elucidate the origins of layering, which is hypothesized to be due to physical aging of the surface layer at low deposition temperatures. It is also important to note that in these inherently anisotropic films, layering and orientation may play different roles if the mechanics are studied in other directions, which should be explored using other techniques than nanoindentation.

Materials and Methods

Materials. Figure 1A shows the structure of 9-(3,5-di(naphthalen-1-yl)phenyl)anthracene (α , α -A) and 9-(3,5-di(naphthalen-1-yl)phenyl) phenanthrene (α , α -Phen) molecules, which were synthesized as described in our previous work. The glass transition temperatures (T_g) of these molecule, as determined by Differential Scanning Calorimetry (DSC), are $T_{g,-A} = 361 \pm 2$ K and $T_{g,-Phen} = 362 \pm 5$ K, respectively. As reported in our previous work, the A-diarylbenzene bond in α , α -A has a higher barrier of dihedral rotation compared to the Phen-diarylbenzene

bond in α , α -Phen. The equilibrium angle of this dihedral bond in α , α -A is also larger than the corresponding bond in α , α -Phen. As such, at low temperatures α , α -A has a spherical shape, while the α , α -Phen is ellipsoidal, α as schematically shown in Figure 1A.

Sample preparation. For each molecule, $0.8 - 1 \mu m$ films were prepared by physical vapor deposition (PVD) from a thermal evaporation source, using a custom vacuum chamber with a base pressure of $\sim 10^{-7}$ Torr (Figure 1B, details in our previous publications 25,53). The molecules were deposited onto silicon substrates (Virginia Semiconductor) bridged across two independently temperature-controlled copper sample holders, and secured on each side using Apiezon PFPE 501 grease and a strong clamp to ensure good thermal contact. This resulted in a gradient of T_{dep} during each deposition. The range of temperature gradient was set by setting the temperature at each end, between 248 K - 371 K for α , α -A and 249 K - 373 K for α , α -Phen, respectively. The temperature at each point along these temperature-gradient (T-grad) samples were determined based on the Fourier's Law, and calibrated using various calibration standards as well as depositions onto individually temperature-controlled substrates, as detailed in our previous publications. ^{25,53} Given the range of the gradients used here and the accuracy of temperature control at each end, the error in defining T_{dep} at each point across the T-grad sample stage was estimated to be ≤ 4 K (details in our previous publications 25,53). The deposition rate (r_{dep}) was monitored using a quartz crystal microbalance (QCM) and was controlled at $r_{dep} = 0.2 \pm 0.03$ nm/s. This deposition rate was chosen to be consistent with our previous work producing typical stable glasses of these molecules. 25,54

Nanoindentation Experiments. Nanoindentation experiments were performed using a Hysitron TI-950 nanoindenter fitted with a Hysitron Berkovich tip. Sites for indentation were selected at distances 2 mm apart, and 30 indents were performed at each site (Figure 1C), under ambient conditions. These positions were then correlated with the calculated T_{dep} values.

Typical preload-based surface detection schemes during nanoidentation can lead to surface detection errors, which affect the accuracy of the hardness and modulus measurements. A procedure schematically shown in Figure 1D was adopted, which we have recently demonstrated can avoid

surface detection errors. 43 This procedure can be summarized as follows:

- 1. Using the preload detection scheme, the tip approaches the sample until it detects the apparent "surface", which is likely at a depth below the actual specimen surface.
- 2. The tip is then lifted off to a distance of 150 nm away from the apparent surface. This height is chosen because it avoids significant noise upon re-approach.
- 3. The tip is offset laterally by 1 μ m from the original approach location. This distance is chosen to avoid interactions with the surface detection indent.
- 4. The tip is loaded into the sample, using load control, with a constant maximum load chosen such that the maximum displacement into the sample is less than 10% of the total sample thickness. This is a common experimental practice that has been shown⁵⁵ to aid in avoiding effects from the substrate below the sample.
- 5. The tip is held at the maximum load for a period of 10 s and is then unloaded from the sample.

The resulting load-displacement curves (Figure 2) were then analyzed to determine the true surface, after which, the Oliver-Pharr method 56,57 was used to determine the hardness (H) and nanoindentation reduced modulus (E_r). These analyses, along with surface detection error calculations, were performed using a MATLAB code. Relevant equations are detailed in the online Supplementary Information, SI.

Comparisons With Other Structural Properties The measured hardness and modulus were compared with previously measured structural characteristics of vapor-deposited films of α , α –A and α , α –Phen molecules. These properties include the relative density ($\Delta \rho$) and optical birefringence as a function of T_{dep} , measured using spectroscopic ellipsometry, and the extent of molecular layering, measured by grazing incidence wide-angle X-ray scattering (GIWAXS) experiments (details in SI and figures S1-S2). These data are from detailed structural analysis reported in our recent publication. ²⁵

Acknowledgement

This research was primarily supported by the University of Pennsylvania Materials Research Science and Engineering Center (MRSEC) grant DMR-1720530, and partially through the National Science Foundation NSF-DMREF Grant (DMR-1628407). PJW thanks support from the NSF grant CHE-1902509. Also acknowledged is use of the Dual Source and Environmental X-ray Scattering facility operated by the Laboratory for Research on the Structure of Matter at the University of Pennsylvania (NSF-MRSEC DMR-1720530) and Prof. Paul Heiney for his help with GIWAXS experiments. The purchase of this equipment was made possible by an NSF MRI grant (17-25969), an ARO DURIP grant (W911NF-17-1-0282) and the University of Pennsylvania.

Supporting Information Available

The following files are available free of charge.

• Supplementary information: Including analysis and experimental details as well as correlation plots

References

- (1) Swallen, S. F.; Kearns, K. L.; Mapes, M. K.; Kim, Y. S.; McMahon, R. J.; Ediger, M. D.; Wu, T.; Yu, L.; Satija, S. Organic Glasses with Exceptional Thermodynamic and Kinetic Stability. *Science* 2007, 315, 353–357, DOI: 10.1126/science.1135795.
- (2) Zhao, J.; Simon, S. L.; McKenna, G. B. Using 20-million-year-old amber to test the super-Arrhenius behaviour of glass-forming systems. *Nat. Commun.* **2013**, *4*, 1783, DOI: 10.1038/ncomms2809.
- (3) Berthier, L.; Ediger, M. D. Facets of glass physics. *Phys. Today* **2016**, *69*, 40–52, DOI: 10.1063/PT.3.3052.

- (4) Royall, C. P.; Turci, F.; Tatsumi, S.; Russo, J.; Robinson, J. The race to the bottom: approaching the ideal glass? *J. Phys. Condens. Matter* **2018**, *30*, 363001, DOI: 10.1088/1361-648X/aad10a.
- (5) Beasley, M. S.; Bishop, C.; Kasting, B. J.; Ediger, M. D. Vapor-Deposited Ethylbenzene Glasses Approach "Ideal Glass" Density. J. Phys. Chem. Lett. 2019, 10, 4069–4075, DOI: 10.1021/acs.jpclett.9b01508.
- (6) Kearns, K. L.; Krzyskowski, P.; Devereaux, Z.; Kearns, K. L.; Krzyskowski, P.; Devereaux, Z. Using deposition rate to increase the thermal and kinetic stability of vapor-deposited hole transport layer glasses via a simple sublimation apparatus. *J. Chem. Phys.* 2017, 146, 203328, DOI: 10.1063/1.4979814.
- (7) Singh, S.; De Pablo, J. J. A molecular view of vapor deposited glasses. *J. Chem. Phys.* **2011**, *134*, DOI: 10.1063/1.3586805.
- (8) Torres, J. M.; Bakken, N.; Li, J.; Vogt, B. D. Substrate Temperature to Control Moduli and Water Uptake in Thin Films of Vapor Deposited N,N'-Di(1-napthyl)-N,N'-diphenyl-(1,1'-biphenyl)-4,4'-diamine (NPD). *J. Phys. Chem. B* **2015**, *119*, 11928–11934, DOI: 10.1021/acs.jpcb.5b05814.
- (9) Gujral, A.; O'Hara, K. A.; Toney, M. F.; Chabinyc, M. L.; Ediger, M. Structural Characterization of Vapor-Deposited Glasses of an Organic Hole Transport Material with X-ray Scattering. *Chem. Mater.* 2015, 27, 3341–3348, DOI: 10.1021/acs.chemmater.5b00583.
- (10) Tylinski, M.; Chua, Y. Z.; Beasley, M. S.; Schick, C.; Ediger, M. D. Vapor-deposited alcohol glasses reveal a wide range of kinetic stability. *Journal of Chemical Physics* 2016, 145, DOI: 10.1063/1.4966582.
- (11) Qiu, Y.; Antony, L.; de Pablo, J. J.; Ediger, M. D. Photostability can be significantly modulated by molecular packing in glasses. *JACS* **2016**, *138*, 11282–11289, DOI: 10.1021/jacs.6b06372.

- (12) Kearns, K. L.; Still, T.; Fytas, G.; Ediger, M. D. High-Modulus Organic Glasses Prepared by Physical Vapor Deposition. *Adv. Mater.* **2010**, 22, 39–42, DOI: 10.1002/adma.200901673.
- (13) Dalal, S. S.; Ediger, M. D. Molecular orientation in stable glasses of indomethacin. *J. Phys. Chem. Lett.* **2012**, *3*, 1229–1233, DOI: 10.1021/jz3003266.
- (14) Liu, T.; Exarhos, A. L.; Alguire, E. C.; Gao, F.; Salami-ranjbaran, E.; Cheng, K.; Jia, T.; Subotnik, J. E.; Walsh, P. J.; Kikkawa, J. M. et al. Birefringent Stable Glass with Predominantly Isotropic Molecular Orientation. *Phys. Rev. Lett.* 2017, 095502, 1–6, DOI: 10.1103/PhysRevLett.119.095502.
- (15) Ràfols-Ribé, J.; Dettori, R.; Ferrando-Villalba, P.; Gonzalez-Silveira, M.; Abad, L.; Lope-andía, A. F.; Colombo, L.; Rodríguez-Viejo, J. Evidence of thermal transport anisotropy in stable glasses of vapor deposited organic molecules. *Phys. Rev. Materials* 2018, 2, 035603, DOI: 10.1103/PhysRevMaterials.2.035603.
- (16) Cang, Y.; Wang, Z.; Bishop, C.; Yu, L.; Ediger, M. D.; Fytas, G. Extreme Elasticity Anisotropy in Molecular Glasses. *Adv. Funct. Mater.* **2020**, 2001481, 1–8, DOI: 10.1002/adfm.202001481.
- (17) Lin, H.-W.; Lin, C.-L.; Chang, H.-H.; Lin, Y.-T.; Wu, C.-C.; Chen, Y.-M.; Chen, R.-T.; Chien, Y.-Y.; Wong, K.-T. Anisotropic optical properties and molecular orientation in vacuum-deposited ter(9,9-diarylfluorene)s thin films using spectroscopic ellipsometry. *J. Appl. Phys.* 2004, 95, 881–886, DOI: 10.1063/1.1635991.
- (18) Oh-e, M.; Ogata, H.; Fujita, Y.; Koden, M. Anisotropy in amorphous films of cross-shaped molecules with an accompanying effect on carrier mobility: Ellipsometric and sumfrequency vibrational spectroscopic studies. *Appl. Phys. Lett.* **2013**, *102*, 101905, DOI: 10.1063/1.4792746.
- (19) Yokoyama, D.; Sakaguchi, A.; Suzuki, M.; Adachi, C. Horizontal molecular orientation in

- vacuum-deposited organic amorphous films of hole and electron transport materials. *Appl. Phys. Lett.* **2008**, *93*, 173302, DOI: 10.1063/1.2996258.
- (20) Yokoyama, D.; Sakaguchi, A.; Suzuki, M.; Adachi, C. Horizontal orientation of linear-shaped organic molecules having bulky substituents in neat and doped vacuum-deposited amorphous films. *Org. Electron.* **2009**, *10*, 127–137, DOI: 10.1016/j.orgel.2008.10.010.
- (21) Gómez, J.; Gujral, A.; Huang, C.; Bishop, C.; Yu, L.; Ediger, M. D. Nematic-like stable glasses without equilibrium liquid crystal phases. *J. of Chem. Phys.* **2017**, *146*, 054503, DOI: 10.1063/1.4974829.
- (22) Teerakapibal, R.; Huang, C.; Gujral, A.; Ediger, M. D.; Yu, L. Organic Glasses with Tunable Liquid-Crystalline Order. *Phys. Rev. Lett.* **2018**, *120*, 055502, DOI: 10.1103/PhysRevLett.120.055502.
- (23) Dawson, K.; Kopff, L. A.; Zhu, L.; McMahon, R. J.; Yu, L.; Richert, R.; Ediger, M. D. Molecular packing in highly stable glasses of vapor-deposited tris-naphthylbenzene isomers. J. Chem. Phys. 2012, 136, DOI: 10.1063/1.3686801.
- (24) Bagchi, K.; Jackson, N. E.; Gujral, A.; Huang, C.; Toney, M. F.; Yu, L.; De Pablo, J. J.; Ediger, M. D. Origin of Anisotropic Molecular Packing in Vapor-Deposited Alq3 Glasses. *J. Phys. Chem. Lett.* **2019**, *10*, 164–170, DOI: 10.1021/acs.jpclett.8b03582.
- (25) Zhang, A.; Moore, A. R.; Zhao, H.; Wolf, S.; Govind, S.; Jin, Y.; Walsh, P. J.; Riggleman, R. A.; Fakhraai, Z. The Effect of Intramolecular Relaxations on the Structure and Stability of Vapor-Deposited Glasses. *Submitted*
- (26) Dawson, K. J.; Zhu, L.; Yu, L.; Ediger, M. Anisotropic structure and transformation kinetics of vapor-deposited indomethacin glasses. *The Journal of Physical Chemistry B* **2011**, *115*, 455–463, DOI: 10.1021/jp1092916.

- (27) Thoms, E.; Gabriel, J.; Guiseppi-Elie, A.; Ediger, M.; Richert, R. In situ observation of fast surface dynamics during the vapor-deposition of a stable organic glass. *Soft Matter* **2020**, *16*, 10860–10864, DOI: 10.1039/D0SM01916J.
- (28) Zhang, Y.; Fakhraai, Z. Invariant fast diffusion on the surfaces of ultrastable and aged molecular glasses. *Physical review letters* **2017**, *118*, 066101, DOI: 10.1103/PhysRevLett.118.066101.
- (29) Chen, Y.; Chen, Z.; Tylinski, M.; Ediger, M. D.; Yu, L. Effect of molecular size and hydrogen bonding on three surface-facilitated processes in molecular glasses: Surface diffusion, surface crystal growth, and formation of stable glasses by vapor deposition. *J. Chem. Phys.* **2019**, *150*, 024502, DOI: 10.1063/1.5079441.
- (30) Bishop, C.; Li, Y.; Toney, M. F.; Yu, L.; Ediger, M. D. Molecular Orientation for Vapor-Deposited Organic Glasses Follows Rate-Temperature Superposition: The Case of Posaconazole. *The Journal of Physical Chemistry B* **2020**, *124*, 2505–2513, DOI: 10.1021/acs.jpcb.0c00625.
- (31) Bagchi, K.; Ediger, M. D. Controlling Structure and Properties of Vapor- Deposited Glasses of Organic Semiconductors: Recent Advances and Challenges. *J. Phys. Chem. Lett.* **2020**, *11*, 6935–6945, DOI: 10.1021/acs.jpclett.0c01682.
- (32) Moore, A. R.; Huang, G.; Wolf, S.; Walsh, P. J.; Fakhraai, Z.; Riggleman, R. A. Effects of microstructure formation on the stability of vapor-deposited glasses. *PNAS* **2019**, *116*, 5937–5942, DOI: 10.1073/pnas.1821761116.
- (33) Gómez, J.; Jiang, J.; Gujral, A.; Huang, C.; Yu, L.; Ediger, M. D. Vapor deposition of a smectic liquid crystal: highly anisotropic, homogeneous glasses with tunable molecular orientation. *Soft Matter* **2016**, *12*, 2942–2947, DOI: 10.1039/C5SM02944A.
- (34) Tylinski, M.; Beasley, M. S.; Chua, Y. Z.; Schick, C.; Ediger, M. D. Limited surface mobility

- inhibits stable glass formation for 2-ethyl-1-hexanol. *J. Chem. Phys.* **2017**, *146*, 203317, DOI: 10.1063/1.4977787.
- (35) Chen, Y.; Zhu, M.; Laventure, A.; Lebel, O.; Ediger, M. D.; Yu, L. Influence of Hydrogen Bonding on the Surface Diffusion of Molecular Glasses: Comparison of Three Triazines. *J. Phys. Chem. B* **2017**, *121*, DOI: 10.1021/acs.jpcb.7b05333.
- (36) Laventure, A.; Gujral, A.; Lebel, O.; Pellerin, C.; Ediger, M. D. Influence of Hydrogen Bonding on the Kinetic Stability of Vapor-Deposited Glasses of Triazine Derivatives. *J. Phys. Chem. B* **2017**, *121*, 2350–2358, DOI: 10.1021/acs.jpcb.6b12676.
- (37) Zhang, A. Manipulating Glass Structure and Properties Through Surface Mediated Equilibrium. Ph.D. thesis, University of Pennsylvania, 2021.
- (38) Fakhraai, Z.; Still, T.; Fytas, G.; Ediger, M. D. Structural variations of an organic glassformer vapor-deposited onto a temperature gradient stage. *J. Phys. Chem. Lett.* **2011**, *2*, 423–427, DOI: 10.1021/jz101723d.
- (39) Tangpatjaroen, C.; Bagchi, K.; Martínez, R. A.; Grierson, D.; Szlufarska, I. Mechanical Properties of Structure-Tunable, Vapor-Deposited TPD Glass. *J. Phys. Chem. C* **2018**, *122*, 27775–27781, DOI: 10.1021/acs.jpcc.8b09718.
- (40) Bakken, N.; Torres, J. M.; Li, J.; Vogt, B. D. Thickness dependent modulus of vacuum deposited organic molecular glasses for organic electronics applications. *Soft Matter* 2011, 7, 7269–727, DOI: 10.1039/C1SM05732D.
- (41) Qian, Z.; McKenna, G. B. On the extreme depth dependence of the hardness of PDMS rubber: A problem of false surface detection. *J. Polym. Sci. B Polym. Phys.* **2017**, *55*, 30–38, DOI: 10.1002/polb.24147.
- (42) Qian, Z.; Risan, J.; Stadnick, B.; Mckenna, G. B. Apparent Depth-Dependent Modulus and Hardness of Polymers by Nanoindentation: Investigation of Surface Detec-

- tion Error and Pressure Effects. *J. Polym. Sci. B Polym. Phys.* **2017**, *56*, 414–428, DOI: 10.1002/polb.24554.
- (43) Fulco, S.; Wolf, S.; Jakes, J. E.; Fakhraai, Z.; Turner, K. T. Effect of surface detection error due to elastic–plastic deformation on nanoindentation measurements of elastic modulus and hardness. *Mater. Res.* **2021**, *36*, 2176–2188, DOI: 10.1557/s43578-021-00223-4.
- (44) Göken, M.; Kempf, M. Pop-Ins in Nanoindentation The Initial Yield Point. *Zeitschrift für Metallkunde* **2001**, *92*, 1061–1067, DOI: 10.3139/ijmr-2001-0193.
- (45) Liu, T.; Cheng, K.; Salami-Ranjbaran, E.; Gao, F.; Glor, E. C.; Li, M.; Walsh, P. J.; Fakhraai, Z. Synthesis and high-throughput characterization of structural analogues of molecular glassformers: 1,3,5-trisarylbenzenes. *Soft Matter* 2015, 11, 7558–66, DOI: 10.1039/c5sm01044f.
- (46) Dalal, S. S.; Fakhraai, Z.; Ediger, M. D. High-throughput ellipsometric characterization of vapor-deposited indomethacin glasses. *J. Phys. Chem. B* **2013**, *117*, 15415–15425, DOI: 10.1021/jp405005n.
- (47) Vlassak, J. J.; Nix, W. D. Indentation modulus of elastically anisotropic half spaces. *Philos. Mag. A, Phys. Condens. Matter Defects Mech. Prop.* **1993**, *67*, 1045–1056, DOI: 10.1080/01418619308224756.
- (48) Vlassak, J. J.; Nix, W. Measuring the Elastic Properties of Anisotropic Materials By Means of Indentation Experiments. *J. Mech. Phys. Solids* **1994**, *42*, 1223–1245, DOI: 10.1016/0022-5096(94)90033-7.
- (49) Delafargue, A.; Ulm, F. J. Explicit approximations of the indentation modulus of elastically orthotropic solids for conical indenters. *Int. J. Solids Struct.* **2004**, *41*, 7351–7360, DOI: 10.1016/J.IJS0LSTR.2004.06.019.

- (50) Vlassak, J. J.; Ciavarella, M.; Barber, J. R.; Wang, X. The indentation modulus of elastically anisotropic materials for indenters of arbitrary shape. *J. Mech. Phys. Solids* **2003**, *51*, 1701–1721, DOI: 10.1016/S0022-5096(03)00066-8.
- (51) Swadener, J. G.; Rho, J. Y.; Pharr, G. M. Effect of anisotropy on elastic moduli measured by nanoindentation in human tibial cortical bone. *J. Biomed. Mater. Res.* **2001**, *57*, 108–112, DOI: 10.1002/1097-4636(200110)57:1<108::AID-JBM1148>3.0.C0;2-6.
- (52) Wolf, S. E.; Liu, T.; Govind, S.; Zhao, H.; Huang, G.; Zhang, A.; Wu, Y.; Chin, J.; Cheng, K.; Salami-Ranjbaran, E. et al. Design of a homologous series of molecular glassformers. *J. Chem. Phys.* **2021**, *155*, 224503, DOI: 10.1063/5.0066410.
- (53) Jin, Y.; Zhang, A.; Wolf, S. E.; Govind, S.; Moore, A. R.; Zhernenkov, M.; Freychet, G.; Arabi Shamsabadi, A.; Fakhraai, Z. Glasses denser than the supercooled liquid. *PNAS* **2021**, *118*, 1–7, DOI: 10.1073/pnas.2100738118.
- (54) Liu, T.; Cheng, K.; Salami, E.; Gao, F.; Li, C.; Tong, X.; Lin, Y.-C.; Zhang, Y.; Zhang, W.; Klinge, L. et al. The effect of chemical structure on the stability of physical vapor deposited glasses of 1,3,5-triarylbenzene. *J. Chem. Phys.* **2015**, *143*, 084506, DOI: 10.1063/1.4928521.
- (55) Chen, K.-S.; Chen, T.-C.; Ou, K.-S. Development of semi-empirical formulation for extracting materials properties from nanoindentation measurements: Residual stresses, substrate effect, and creep. *Thin Solid Films* **2008**, *516*, 1931–1940, DOI: 10.1016/j.tsf.2007.09.005.
- (56) Oliver, W.; Pharr, G. Measurement of hardness and elastic modulus by instrumented indentation: Advances in understanding and refinements to methodology. *Mater. Res.* **2004**, *19*, 3–20, DOI: 10.1557/jmr.2004.19.1.3.
- (57) Pharr, G.; Oliver, W. Measurement of Thin Film Mechanical Properties Using Nanoindentation. *MRS Bull.* **1992**, *17*, 28–33, DOI: 10.1557/S0883769400041634.